Journal of the Taiwan Institute of Chemical Engineers 104 (2019) 54–64

Contents lists available at ScienceDirect

Journal of the Taiwan Institute of Chemical Engineers

journal homepage: www.elsevier.com/locate/jtice

Free standing Si (Ge) nanowire/Cu nanowire composites as lithium ion battery anodes

Kuan-Ting Chen[1], Wei-Chung Chang[1], Hong-Jie Yang, Chun-Yu Tsai, Sheng-Bor Huang, Hsing-Yu Tuan*

Department of Chemical Engineering, National Tsing Hua University, Hsinchu 300, Taiwan

ARTICLE INFO

Article history:
Received 11 February 2019
Revised 18 July 2019
Accepted 22 July 2019
Available online 24 August 2019

Keywords:
Nanowire
Free standing
Composites
Lithium
Battery

ABSTRACT

Silicon (Si) and germanium (Ge) can alloy with lithium to achieve high theoretical specific capacities (3579 mAh/g for $Li_{15}Si_4$ and 1384 mAh/g for $Li_{15}Ge_4$), which are several times greater than commercial graphite (372 mAh/g). However, they exhibit significant volume and crystal structural change during cycling processes, leading to structural pulverization and loss of electrical conduction paths between individual active materials and current collector. We report a non-carbon based free standing electrodes fabricated by directly mixing Si and Ge nanowires with Cu nanowires as lithium ion battery anodes. The one dimensional nanostructure of Si (Ge) and Cu provide good charge transport along their length and many contact points were formed between NWs after annealing process. The nanowire composites have several advantages compared to the conventional electrode that slurry materials are coated on a metal foil. For example, the weight is lighter than conventional electrodes because it does not need a current collector and is fabricated without any additives, and binders. Moreover, the space among the nanowires can accommodate the volume contraction of Si (Ge) during alloying and dealloying process and enhance the electrolyte penetration.

1. Introduction

Lithium ion batteries (LIBs) are one of the most important rechargeable batteries and have become widely used in consumer electronics, transportation, electric vehicles, and so forth [1–3]. In order to develop LIBs having high energy density, *group* IVA elements, silicon (Si) and germanium (Ge), that can alloy with lithium have received tremendous interest because of their high theoretical specific capacity (3579 mAh/g for $Li_{15}Si_4$ and 1384 mAh/g for $Li_{15}Ge_4$), which are several times greater than graphite (372 mAh/g) [4–6]. However, these alloy-type anode materials exhibit significant volume and crystal structural change during alloying and dealloying processes, leading to structural pulverization of Si (Ge) anode material, loss of electrical conduction paths between individual active materials and current collector, thus continue to form solid electrolyte interphase (SEI), and results in consequent serious capacity fading upon cycling [7].

To overcome this issue, several strategies had been proposed. One effective way is to employ nanomaterials as active materials. Using nanomaterials as anodes can offer many advantages such as providing small diffusion length for Li transport and alleviating the large mechanical strain during lithiation and delithiation, and hence improving the stability of nanostructures-based anodes [8,9]. Nowadays, a variety of Si (Ge) nanostructures-based anodes have been reported to show their ability to tolerate strain relaxation during cycling [10–15]. Silicon nanoparticles with diameters less than 20 nm as anode materials shows size-dependent lithium-storage properties [11]. Germanium nanotubes anodes prepared by a Kirkendall effect exhibit extraordinary high rate capability and excellent capacity retention. Later on, Si nanotubes were also prepared by decomposition of a silicon precursor in an alumina template and etching, showing superior capacity retention at 5 C. 3D porous Ge nanoparticles assemblies prepared by etching SiO_2 particles can show almost 99% of its capacity after 100 cycles. One dimensional Si (Ge) nanowires (NWs) offer short Li diffusion path in the radial direction and good charge transport along their length which can be made into binder free anode electrode structures [16]. For example, Chan et al. reported a binder free Si NWs anode electrode structures by growing Si NWs directly on the stainless steel current collector which exhibited excellent electrochemical performance [10]. Zhang et al. developed a composite anode of Cu/Si/Ge nanowire arrays grown on a Ni foam substrate, exhibited an excellent rate performance with long-cycle stability [17]. However, this kind of anode structures have low mass

* Corresponding author.
E-mail address: hytuan@che.nthu.edu.tw (H.-Y. Tuan).
[1] These authors contributed equally to this work.

https://doi.org/10.1016/j.jtice.2019.07.014
1876-1070/

loading limitations due to restricted growth on a substrate. Germanium nanowires-based carbon composites show improved capacity retention *via* porous carbon's synergistic effect, but carbon occupy large weight percentage in the electrode [15]. Recently, two-dimensional nanosheets of germanane have been investigated as another type of lithium-ion anode materials, but its high rate capacity was relatively low [18]. Liu et al. report a facile sol-gel synthesis of monodisperse SiO_x/C microspheres with tunable size and well-controlled carbon content and demonstrate high capacity and excellent cycling stability in lithium storage [19], which demonstrates that silicon oxides is a promising family of anode materials for lithium-ion batteries [20].

In a typical process for fabricating LIB electrodes, slurry composed of binder, conducting additive, active materials, and solvent are coated on a metal current collector. Nanostructuring of materials inspires new electrode structure design. Free standing electrodes made by carbon nanomaterials (carbon nanotubes, carbon fiber, and graphene) can be directly used as electrodes with characteristic of lightweight, high flexibility and good conductivity [21,22]. But the carbon based free standing electrodes suffer the same problem for the purpose of LIBs with high energy density. Several reports attempt to increase the capacity of the carbon based free standing electrodes by loading or coating high capacity nanomaterials on carbon nanotubes or graphene [23–26]. To the best of our knowledge, there is only a few reports about free standing fabric electrodes which is not made by carbon based nanomaterials. For example, Si NW fabric anode electrodes produced by SFLS mechanism and followed by thermal annealing show anode capacities > 800 mAh/g at 0.05 C and 20 cycles [24,27]. We attributed this low anode capacities is due to the low conductivity of Si itself without adding other conducting agent. Recently, bilayer Ge/Cu nanowire mesh electrodes exhibited a high specific capacity of 830 mAh/g at 1 C after 1000 cycles, which shows that addition of conducting agent into Si (Ge)-based fabric electrodes is needed [28].

Therefore, compared to carbon-based approaches, how to enhance electrochemical performance of Si (Ge) anodes using non-carbon based approach is relatively unknown. Herein, we present non-carbon based free standing NW fabric anode electrodes constructed by highly conductive Cu NWs with Si (Ge) NWs and, and their electrochemical properties as LIBs anodes are presented. The main reason for adding Cu NWs is to increase the electronic conductivity of the whole fabric anode electrodes. The one dimensional nanostructure of Si (Ge) and Cu not only provide good charge transport along their length but also offer many contact points between NWs. A proper weight percentage of Cu NWs in the NW fabric is the key point to improve electrochemical performance of the Si (Ge) NW fabric anode electrodes and still maintain physical connections between NWs. The weight of whole electrode is significantly lighter than conventional electrodes made by slurry coating on metal foils due. Moreover, the space among the NWs can accommodate the volume contraction of Si (Ge) NWs during alloying and dealloying process and enhance the electrolyte penetration for fast Li-ion diffusion.

2. Experimental section

2.1. Materials

2.1.1. Chemicals

Silicon nanowires, hydrogen tetrachloroaurate(III) trihydrate (99.9%), tetraoctylammonium bromide (98%), sodium borohydride (98.0%), toluene (99.9%), anhydrous toluene (99.8%), 1-dodecanethiol (98%), absolute ethanol (99.8%), copper(I) chloride (CuCl, 99.995%), hydrofluoric acid (48 wt% in H_2O), polydispersed silicon nanowires, and oleylamine (OLA, 70%) were purchased from Aldrich. Diphenylgermane (DPG, 95%) was purchased from Gelest.

2.2. Methods

2.2.1. Synthesis of Ge nanowires

Ge NWs reactions were synthesized according to the literature method [29]. The inlet of a 10 mL titanium (Ti) grade 2 reactor was connected to a stainless steel (1/16″ i.d.) tubing *via* a LM-6 HIP (High Pressure Equipment Co.) reducer and an injector valve (Valco) equipped with a 5 mL injection loop *via* a 1/16″ stainless steel tubing. The temperature of the reactor was covered with heating tape and insulation tape, and controlled by a temperature controller. The system pressure was pressurized and monitored by a high-pressure liquid chromatography pump (Lab Alliance, series 1500) and a digital pressure gauge, respectively.

For a typical Ge NWs synthesis, a stock solution of 170 µL DPG and 170 µL dodecanethiol-coated Au nanoparticle solution (1 mg/1 mL dispersed in toluene, Au nanoparticles were prepared according to the literature [30]) in 5 mL anhydrous toluene was prepared in an Ar-filled glove box. Prior to the synthesis, the reactor was transferred into the glove box to eliminate oxygen and then was brought out from the glove box. Next, the reactor was heated to 420 °C and pressurized to 500 psi. The precursor solution was injecting into a 5 mL loading loop and delivered by the HPLC pump with an injection rate of 0.55 mLmin^{-1}. After injection time of 12 min, another precursor solution was injecting into the 5 mL loading loop again for another 12 min and with three successive injections. When the reaction ended, the valve, HPLC pump, and heater were closed. Water bath was used to cool the reactor until it reached room temperature. The Ge NWs obtained from reactor were purified by centrifuged at 8000 rpm for 5 min with toluene and repeated three times.

2.2.2. Alkanethiol reactions of Si and Ge nanowires

Si (Ge) NWs were immersed in aqueous 5% HF for 5 min and then washed with anhydrous methanol. Next, the NWs were dried in vacuum for 10 min, followed by quickly transferred to a Schlenk line under Ar atmosphere. 10 mL of 1-dodecanethiol was added to immerse NWs and heated to 80 °C for 24 h. Afterwards, the NWs product was centrifuged at 8000 rpm for 5 min with toluene and ethanol at a 1: 1 volume ratio. The washing procedure was repeated twice to remove undesired materials. The thiol-passivated Si (Ge) NWs were stored in glove box for further use.

2.2.3. Synthesis of Cu nanowires

Cu NWs were prepared according to the article with a slight modification [28]. In a typical reaction, 0.3 g CuCl in a 30 mL of OLA solution in a three-necked flask was prepared inside Ar-filled glove box and then brought out from the glove box, followed by connected to a Schlenk line under Ar atmosphere. The mixture solution was heated to 110 °C with stirring for 1 h and then to 260 °C for another 1 h. When the reaction ended, the Cu NWs were washed by addition of 30 mL toluene into the reaction mixture with centrifugation at 8000 rpm for 5 min and repeated twice. The precipitated Cu NWs were stored in glove box for further use.

2.2.4. Fabrication of free standing nanowire fabric

The free standing NW fabric was made by air-drying toluene solution of dispersed Si (Ge) NWs and Cu NWs (total weight of nanowires is about 1.6 mg) in a Teflon (polytetrafluoroethylene, PTFE) mold with size of 10 mm (length) × 10 mm (width) × 5 mm (height) and then was removed by careful peeling the NW fabric from the Teflon mold. For Si NW/Cu NW fabric fabricated at weight ratio of 1: 1, 1: 3, and 1: 7 (Si: Cu) were named S1, S2, and S3, respectively. For Ge NW/Cu NW fabric fabricated at weight

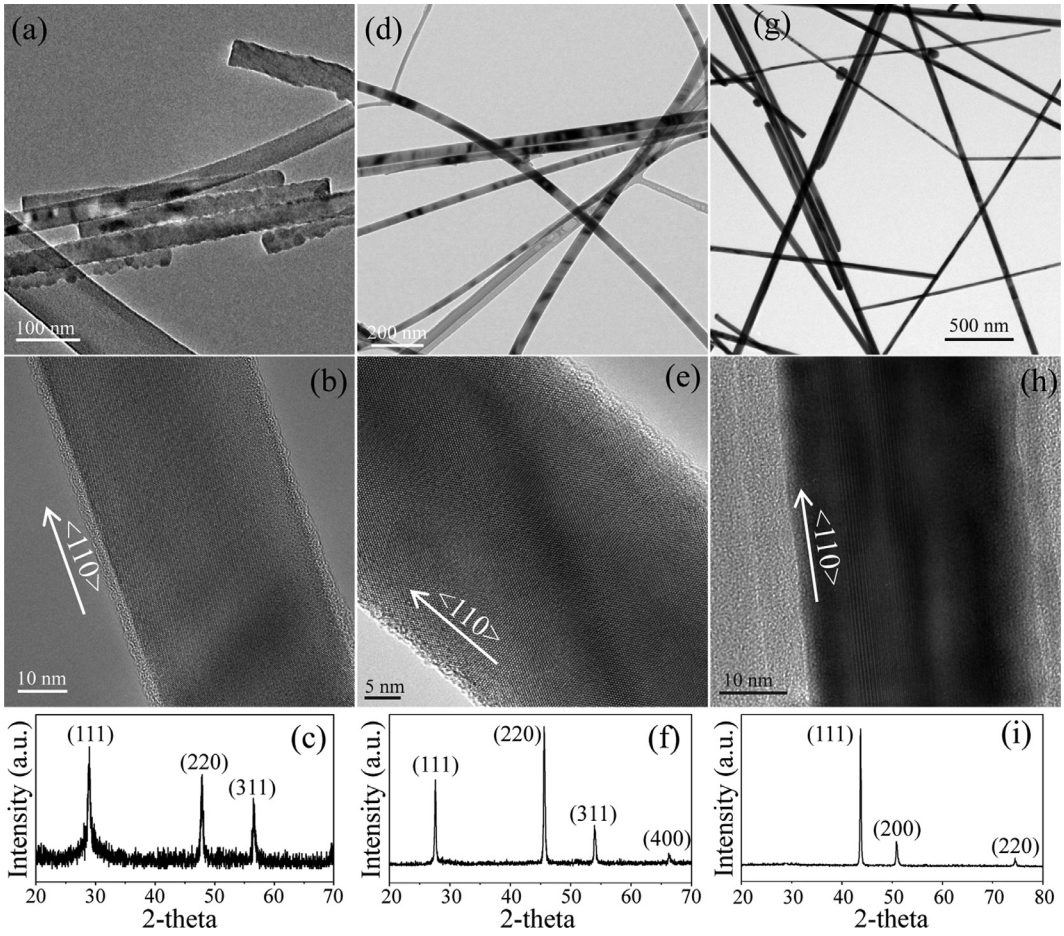

Fig. 1. TEM images, HRTEM images, and XRD patterns of (a)–(c) Si, (d)–(f) Ge, and (g)–(i) Cu nanowires.

ratio of 1: 1, 3: 1, and 1: 0 (Ge: Cu) were named G1, G2, and G3, respectively. The free standing Si (Ge) NW/Cu NW fabric was directly used as LIB anode electrodes without conventional slurry preparation steps. The free standing NW fabrics composed of different weight percentage of Si (Ge) NWs and Cu NWs were annealed at 100 °C, 300 °C, or 500 °C under a pressure of 0.1 torr and Ar (150 sccm)/H_2 (50 sccm) gas flow for 2 h.

2.2.5. Characterization

Scanning electron microscopy (SEM) images were using a HITACHI-U8010 FESEM operating at 10 kV or 15 kV accelerating voltage equipped with an energy dispersive spectroscopy (EDS) detector. Transmission electron microscopy (TEM) and HRTEM images were performed (JEOL JEM 2100F) operating at accelerating 200 kV. TEM samples were prepared by drop-casting the NW solution (in toluene) onto a 200 mesh lacey carbon-coated copper grid. X-ray diffraction (XRD) pattern was prepared by drying NW solution on glass substrates. XRD pattern was carried out on a Rigaku, Ultima IV X-ray diffractometer using Cu–Ka radiation operated at 40 kV and 20 mA ($\lambda = 0.15418$ nm).

2.2.6. Electrochemical characterization

The weight of the fabric was measured using a microbalance with 0.1 μg resolution (Sartorius SE2). The coin-type half-cells (CR2032) were assembled in an Ar-filled glove box and prepared out of free standing NW fabric as the working electrode, Li metal foil as the counter electrode, and microporous polyethylene separator soaked in electrolyte. The electrolyte solution was 1 M $LiPF_6$ in 3: 7 (v/v) fluoroethylene carbonate/dimethyl carbonate (FEC/DMC). No binders or conducting carbon were used. Cycle capacity of the free standing NW fabric was evaluated using a Maccor Series 4000 Battery Test System instrument in a voltage window of 1.5–0.01 V. The electrode capacity was calculated based on the weight of the active materials. Cyclic voltammetry tests were carried using Biologic VMP3 instruments between voltage range of 1.5 and 0.01 V at a scanning rate of 0.1 mV s^{-1}.

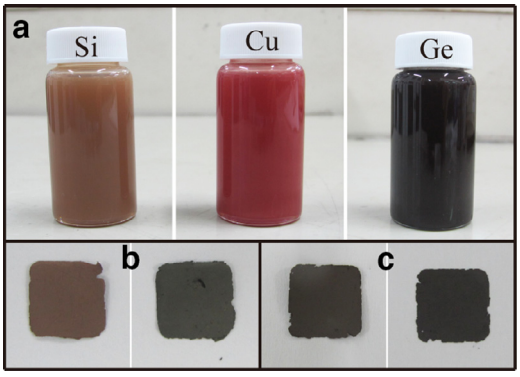

Fig. 2. (a) Photographies of Si, Cu, and Ge NW inks. (b) Photographies of Si NW/Cu NW (1/3, w/w) fabric before (left) and after (right) annealing at 500 °C, and (c) Ge NW/Cu NW (3/1, w/w) fabric before (left) and after (right) annealing at 300 °C.

3. Result and discussion

Fig. 1 display the TEM images, HRTEM images, and XRD patterns of Si, Ge, and Cu NWs. TEM images (Fig. 1(a), (d), and (g)) show the materials used to make NW fabric are mainly composed

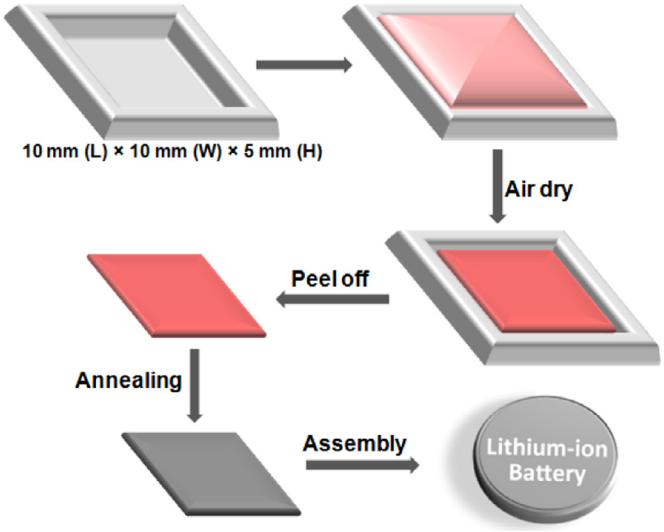

Fig. 3. Schematic diagram of the process of NW fabric fabrication.

of a large quantity of NWs with the diameter mostly ranging from 15 to 35 nm for Si NWs, 25 to 55 nm for Ge NWs, and 45 to 83 nm for Cu NWs. After statistical calculations, Si, Ge, and Cu NWs have a mean diameter of 32 nm, 45 nm, and 68 nm with typical about 1 μm, 12 μm, and 10 μm in length, respectively. It is worth noting that the length of Si NWs bought from the company is significantly shorter than the Ge and Cu NWs that were produced in our lab. Fig. 1(c), (f), and (i) shows the XRD patterns of Si, Ge, and Cu NWs, respectively, confirming the crystalline diamond cubic structure of Si (PDF Card No. 27-1402), crystalline diamond cubic structure of Ge (PDF Card No. 04-006-2620), and crystalline face centered cubic structure of Cu (PDF Card No. 03-1018). Further detailed crystal structures were investigated by HRTEM. Fig. 1(b), (e), and (h) shows lattice-resolved HRTEM images of Si, Ge, and Cu NWs, respectively. The growth direction of Si and Ge NWs are both ⟨110⟩ with single crystallinity, Cu NWs also grew along ⟨110⟩ direction but exhibiting clean [111] twin plane oriented parallel to its growth direction which confirms the five-twinned structure in the Cu NWs and is consistent with previous report [31].

In order to generate uniformly dispersed NW inks for the preparation of NW fabric, the dispersibility of NWs in organic solvent needed to be improved, hence surface passivation of Si and Ge NWs had performed (Cu NWs is already capped by OLA after synthesis). Fig. 2(a) shows the Si, Ge, and Cu NW solutions (dispersed in toluene) displaying unearthed, dark brown, and red brown color, respectively. The dispersibility of Ge and Si NWs is enhanced after alkanethiol reactions and these NWs are still well dispersed in toluene after 2 h indicating that the surface of Ge and Si NWs is indeed well capped by organic ligands. Fig. 2(b) and (c) shows the photographies of Si NW/Cu NW fabric and Ge NW/Cu NW fabric made by drying NW inks solution in a Teflon template (Fig. 3 shows the fabrication process). Unlike bulk Si (Ge), it is inherently brittle. Si (Ge) semiconductor nanowire fibers and fabrics made by this method are flexible and bendable. Videos S1 and S2 observe the fabric's flexible properties and mechanical softness *via* mechanical manipulation. From SEM images (Fig. 4(a) and (b)), the

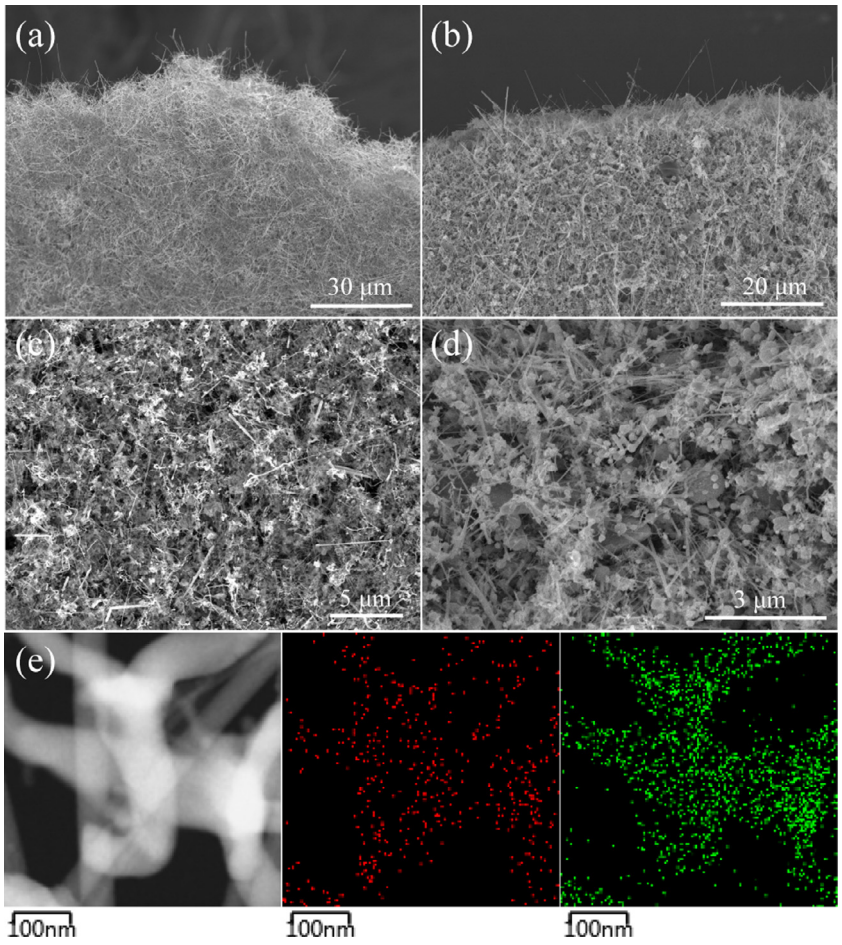

Fig. 4. SEM images of Si NW/Cu NW (weight ratio of 1/3) fabric (a) before and (c) after annealing at 500 °C, and Ge NW/Cu NW (weight ratio of 3/1) fabric (b) before and (d) after annealing at 300 °C.

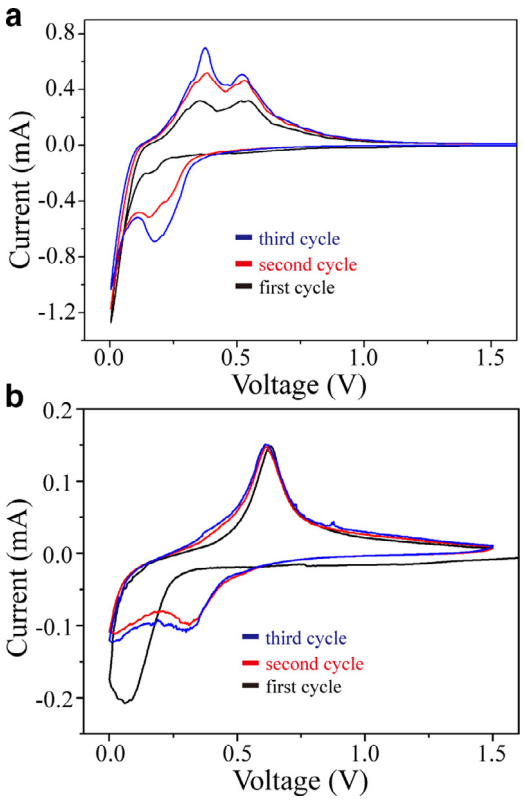

Fig. 5. Cyclic voltammetry (CV) characterizations of (a) S2 electrodes annealing at 500 °C and (b) G2 electrodes annealing at 300 °C in the voltage range of 0.01–1.5 V (versus Li/Li+).

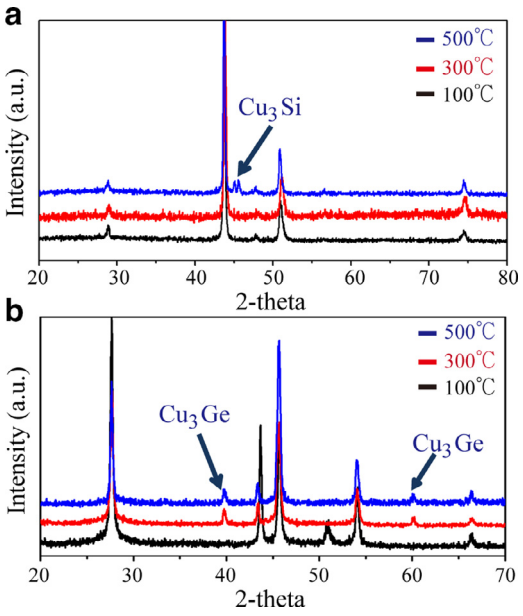

Fig. 6. XRD patterns of (a) S2 and (b) G2 electrodes annealing at 100 °C, 300 °C, and 500 °C.

Si NW/Cu NW fabric and Ge NW/Cu NW fabric are mainly composed of randomly oriented NWs. SEM image with corresponding (Figs. S1 and S3) EDS mapping images of Si (Ge) and Cu show a uniform distribution of Si (Ge) and Cu signals indicating that the Si (Ge) NWs and Cu NWs are evenly distributed in the NW fabric. After annealing process, the color of the Si NW/Cu NW fabric and Ge NW/Cu NW fabric was changed significantly after high temperature annealing (Fig. 2(b) and (c), 500 °C for Si and 300 °C for Ge). Some NWs still maintain their straight wire shape, some NWs become kinking, and many nanoparticles with size about 100–200 nm start appear. After annealing, the Si and Cu elements are still well distributed throughout the NW fabric which is confirmed by SEM images (Fig. 4(c) and (d)) and EDS mapping (Fig. 4(e) and Figs. S1–S3).

To analyze the electrochemical properties of Si NW/Cu NW fabric electrodes and Ge NW/Cu NW fabric electrodes, cyclic voltammetry (CV) was performed on half cells for a S2 electrode annealing at 500 °C and a G2 electrode annealing at 300 °C for the first cycle with the subsequent cycles in the voltage range of 0.01–1.5 V (versus Li/Li^+). For a S2 electrode (Fig. 5(a)), a cathodic peak began at a 0.2 V and became large below 0.1 V during lithiation reactions corresponding to the conversion of crystalline Si to the amorphous Li_xSi phase. Upon delithiation, two anodic peaks at 0.34 and 0.52 V correspond to the delithiation of amorphous Li_xSi to amorphous Si. The intensity of all current peaks increases with cycling due to gradual activation of Si to react with lithium which is consistent with previous Si nanostructures anodes [32,33]. For the G2 electrode (Fig. 5(b)), the peaks at 0.08–0.450 V are assigned to the formation of the Li–Ge alloy during lithiation reactions and the peaks located at 0.58 V can be attributed to the phase transition of Li_xGe to Ge [34,35]. In addition, no extra peaks were appeared in the CV measurements of S2 and G2 electrodes and the current density in the CV profile of net Cu NW fabric is about two orders of magnitude lower than S2 electrodes (Fig. S5). These results both indicate that the Cu NWs only act as a conducting additive for the free standing NW fabric electrode.

To study the effect of the annealing temperatures (100 °C, 300 °C, and 500 °C) on S2 and G2 anode electrodes, XRD measurements had performed. For a S2 electrode (Fig. 6(a)), display diffraction peaks that belong to diamond cubic structure of Si and face centered cubic structure of Cu. However, additional peak at about 45° assigned to Cu_3Si phase appears when the annealing temperature reached 500 °C. For G2 electrodes (Fig. 6(b)), diffraction peaks assigned to diamond cubic structure of Ge and face centered cubic structure of Cu appear in all G2 electrodes and Cu_3Ge phase forms when the annealing temperature exceeds 300 °C. The XRD patterns (Fig. 6) and SEM images (Fig. 4) show the annealing process leading to intensive Cu diffusion into the Si (Ge) NWs to form copper silicide (germanide) with the destruction of the nanowire shape (kinking) and formation of irregular particles. We believe that this phenomenon mainly occur at the junction between Si (Ge) NWs and Cu NWs.

The effect of the annealing temperature on the electrochemical performance of S2 and G2 electrodes were tested by galvanostatic discharge/charge voltage profiles and cycling performance at the 0.05 C rate for Si and 0.1 C rate for Ge from 1.5 to 0.01 V using a 1 M $LiPF_6$ electrolyte solution (FEC/DEC), since FEC is a well-known chemical agent for the formation of superior solid-electrolyte interphase (SEI) layer on the surface of Si and Ge nanostructure anode electrodes [36,37]. The first discharge and charge voltage profiles of a S2 electrode at annealing temperature of 100 °C, 300 °C, and 500 °C are shown in Fig. 7(a). All voltage profiles exhibit a long flat plateau during charge (crystalline Si reacted with Li to form amorphous Li_xSi) and two plateaus during discharge which are consistent with the CV measurements. For the S2 electrode annealing at 100 °C, 300 °C, and 500 °C, the first charge and discharge capacities are 2374 mAh/g and 665 mAh/g giving an initial Coulombic efficiency of 28.0%, 3829 mAh/g and 3214 mAh/g giving an initial Coulombic efficiency of 83.9%, and 3139 mAh/g and 2587 mAh/g giving an initial Coulombic efficiency of 82.4%, respectively. Fig. 7(b) shows the cycle performances of a S2 electrode at annealing temperature of 100 °C, 300 °C, and 500 °C. The capacities

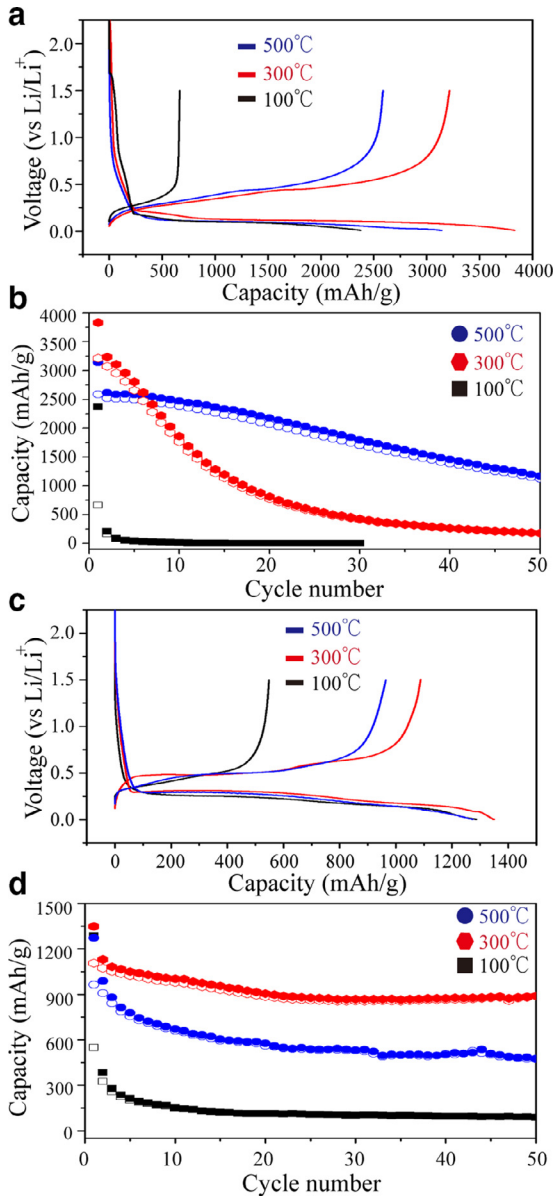

Fig. 7. First galvanostatic discharge/charge voltage profiles and cycling performance of (a) and (b) S2 and (c) and (d) G2 electrodes annealing at 100 °C, 300 °C, and 500 °C.

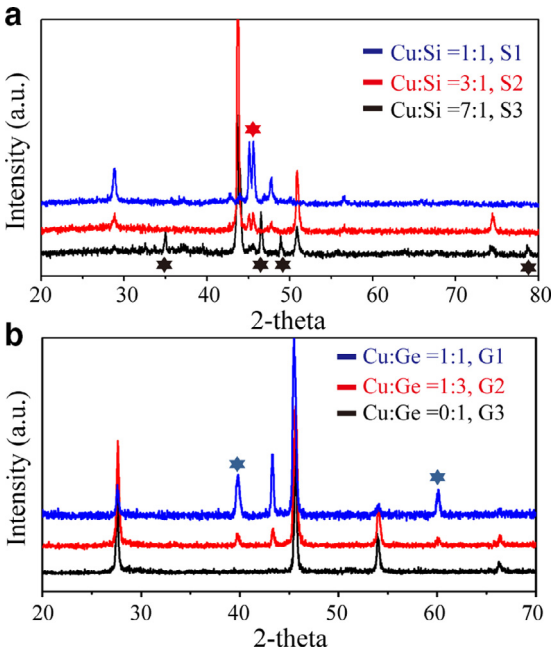

Fig. 8. (a) XRD patterns of S1, S2, and S3 electrodes annealing at 500 °C. (b) XRD patterns of G1, G2, and G3 electrodes annealing at 300 °C. Black star: $Cu_{15}Si_4$, red star: Cu_3Si, blue star: Cu_3Ge. (For interpretation of the references to color in this figure legend, the reader is referred to the web version of this article.)

of the S2 electrode annealing at 100 °C rapid degrade under 100 mAh/g just within three cycle and the cyclability of the S2 electrode annealing at 500 °C exhibits charge and discharge capacities of 1168 and 1123 mAh/g, respectively, at the 50 cycles. These results indicate that the cyclability and initial Coulombic efficiencies (from 28.0% to 82.4%) can be improved with increasing annealing temperature. Fig. 7(c) and (d) represent the 1st galvanostatic discharge/charge voltage profiles and cycle behavior of a G2 electrode at annealing temperature of 100 °C, 300 °C, and 500 °C, it can be seen that the G2 electrode electrodes deliver initial charge and discharge capacities of 1286 mAh/g and 548 mAh/g corresponding to the Coulombic efficiency of 42.6% at annealing temperature of 100 °C, initial charge and discharge capacities of 1348 mAh/g and 1107 mAh/g corresponding to the Coulombic efficiency of 82.1% at annealing temperature of 300 °C, and initial charge and discharge capacities of 1272 mAh/g and 964 mAh/g corresponding to the Coulombic efficiency of 75.7% at annealing temperature of 500 °C. From Fig. 7(d), the G2 electrode annealing at 300 °C show the best reversible capacity of 889 mAh/g with capacity retention of ~80.3% and the G2 electrode annealing at 100 °C shows the worst reversible capacity of 87 mAh/g with capacity retention of ~15.8% at 50 cycles. The irreversible capacity of all S2 and G2 electrodes can be attributed to the formation of SEI layer and irreversible reaction during cycling. We attributed that the better cycling performance and initial Coulombic efficiency of NW fabric electrodes after annealing are due to the better electronic conductivity of individual NW (eliminating the surface ligands) and good contact point formation between NWs (Cu_3Si and Cu_3Ge). However, For Ge based electrodes, when the annealing temperature increases to 500 °C (G2 electrode), the initial Coulombic efficiency (75.7%) and capacity retention (48.9%) decrease compared with annealing at 300 °C. We speculate that the wire shape seriously destroyed accompanying with formation of irregular particles resulting in the loss of the three-dimensional interconnectivity structure is the main reason. A high annealing temperature (*e.g.*, 500 °C) leads to decreasing the number of intersection between the NWs, so hindered the electron transfer, resulting in poor initial Coulombic efficiency and capacity retention compared with 300 °C.

In addition to the effect of annealing temperature on the electrochemical performance, we also study the effect of fabric composition (Si (Ge) and Cu weight ratio) on the electrochemical performance. Firstly, structural characterizations were investigated by XRD measurements to understand the crystal structural change of NW fabric electrodes made by different weight ration of Si(Ge) and Cu NWs after annealing (500 °C for Si NW based fabric and 300 °C for Ge NW based fabric). For S1, S2, and S3 electrodes (Fig. 8(a)), they both present Si, Cu, and Cu_3Si phases (red star) and the intensity of diffraction peaks at about 28° assigned to Si decrease when the loading mass of Cu NWs increase. In addition, $Cu_{15}Si_4$ phase (black star) would appear when the weight ration of Cu NWs/Si NWs for making NW fabric electrode is 7 (S3 electrode). For G1 and G2 electrodes (Fig. 8(b)), Ge, Cu, and Cu_3Ge (blue star) can be detected in all samples and the intensity of Cu and Cu_3Ge enhance when the loading mass of Cu NWs in the NW fabric increase. Fig. 9 shows the voltage profiles versus lithium and cy-

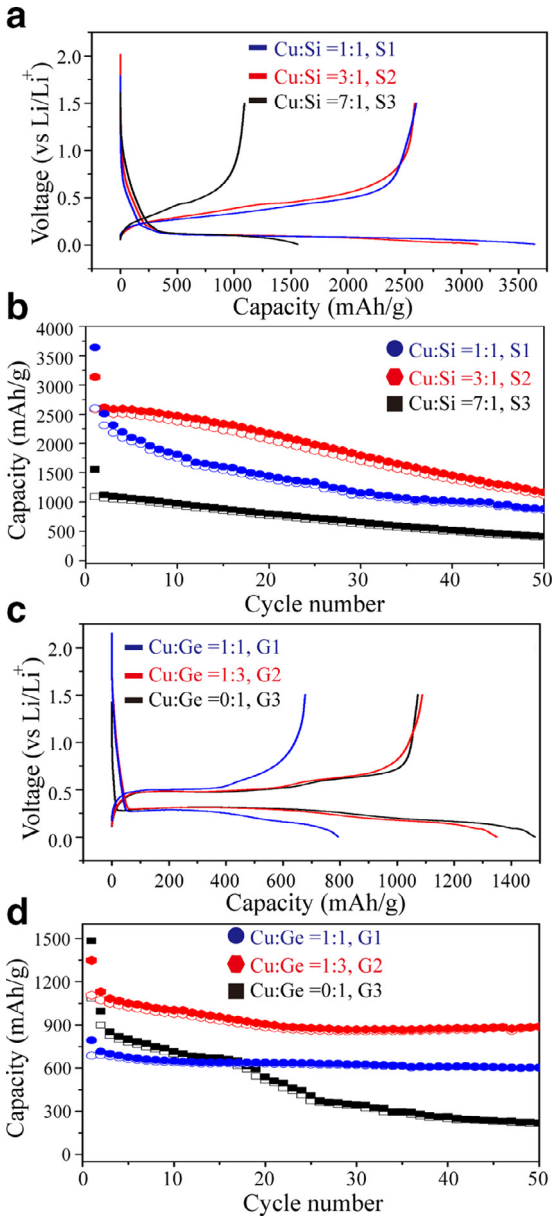

Fig. 9. (a) First galvanostatic discharge/charge voltage profiles and (b) cycling performance of S1, S2, and S3 electrodes annealing at 500 °C. (c) First galvanostatic discharge/charge voltage profiles and (d) cycling performance of G1, G2, and G3 electrodes annealing at 300 °C.

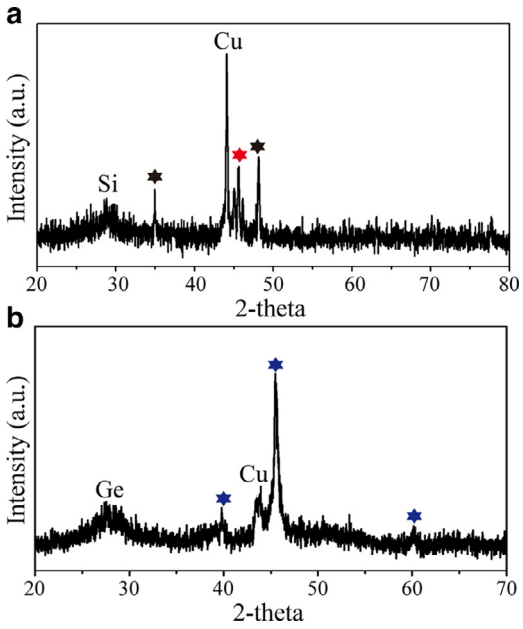

Fig. 10. (a) XRD patterns of S3 electrodes annealing at 500 °C after 5 cycles. (b) XRD patterns of G2 electrodes annealing at 300 °C after 5 cycles. Black star: $Cu_{15}Si_4$, red star: Cu_3Si, blue star: Cu_3Ge. (For interpretation of the references to color in this figure legend, the reader is referred to the web version of this article.)

cling performance of S1, S2, and S3 electrodes annealing at 500 °C, and G1, G2, and G3 electrodes annealing at 300 °C. For Si NW/Cu NW fabric electrodes, they have an initial charge and discharge capacity of 3639 mAh/g and 2599 mAh/g, respectively, with Coulombic efficiency of 71.4% and capacity retention of 33.1% at 50 cycles for S1, 3139 mAh/g and 2587 mAh/g, respectively, with Coulombic efficiency of 82.4% and capacity retention of 43.4% at 50 cycles for S2, and 1557 mAh/g and 1090 mAh/g, respectively, with Coulombic efficiency of 70.0% and capacity retention of 36.5% at 50 cycles for S3. For Ge NW/Cu NW fabric electrodes, the initial charge and discharge capacity are 793 mAh/g and 686 mAh/g, respectively, giving Coulombic efficiency of 86.5% with capacity retention of 87.4% at 50 cycles for G1, 1348 mAh/g and 1107 mAh/g, respectively, giving Coulombic efficiency of 82.1% with capacity retention of 80.3% at 50 cycles for G2, and 1286 mAh/g and 548 mAh/g, respectively, giving Coulombic efficiency of 42.6% with capacity retention of 15.8% at 50 cycles for G3. It is obvious that the initial charge and discharge capacity is found to decrease in both cases (Si and Ge) with increasing the loading mass of Cu NWs. The situation is related with the formation of copper silicide and copper germanide which are electrochemically inactive materials [38–41]. We have measured the XRD patterns of S3 and G2 electrodes after 5 cycles. From the XRD patterns (Fig. 10), we can know that the crystalline Si and Ge become amorphous after 5 cycles. Cu, copper silicide, and copper germanide still maintain their crystal structure after 5 cycles indicating that they do not react with Li during cycling. Therefore, more copper silicide (germanide) would form when the loading mass of Cu NWs increases, leading to reducing the amount of electrochemically active materials (Si and Ge) and lower initial charge and discharge capacity. The electrochemical performance of NW fabric electrodes would present the best when the loading mass of Cu NWs is appropriate. For example of Si based electrodes, S3 electrode (weight ratio of Cu/Si = 7) contains more Cu NWs than S2 electrode (weight ratio of Cu/Si = 3), however the initial Coulombic efficiency and cycle stability of S3 electrode is worse than S2. This phenomenon can be explained as described above, the shape of NWs is seriously damaged and lots of irregular particles are formed when the loading mass of Cu NWs is too much, leading to an electrical disconnection between NWs and hindering electron transfer. For Ge based electrodes, the initial Coulombic efficiency and cycle stability of the G1 electrode (weight ratio of Cu/Ge = 1) is better than the G2 (weight ratio of Cu/Ge = 1/3), however the capacity would significantly reduced when too much copper germanide forms. In addition, compared with Si-based electrodes, Ge-based electrodes have superior capacity retention and the amount of Cu NWs needed for improving the cycle stability is relatively low. The main reasons are due to Ge having a higher diffusivity of lithium ion (400 times greater than Si) and high electrical conductivity (10^4 times greater than Si). The Nyquist plot with a semicircle at medium frequency region and a straight line at low frequency region were illustrated in Fig. S6. As frequency decreases, there is a semicircle called charge transfer resistance, indicating that lithium ions passing through the SEI film and charge transfer between electrolyte and active material. Both Si (Ge)/Cu nanowires after cycling showed the

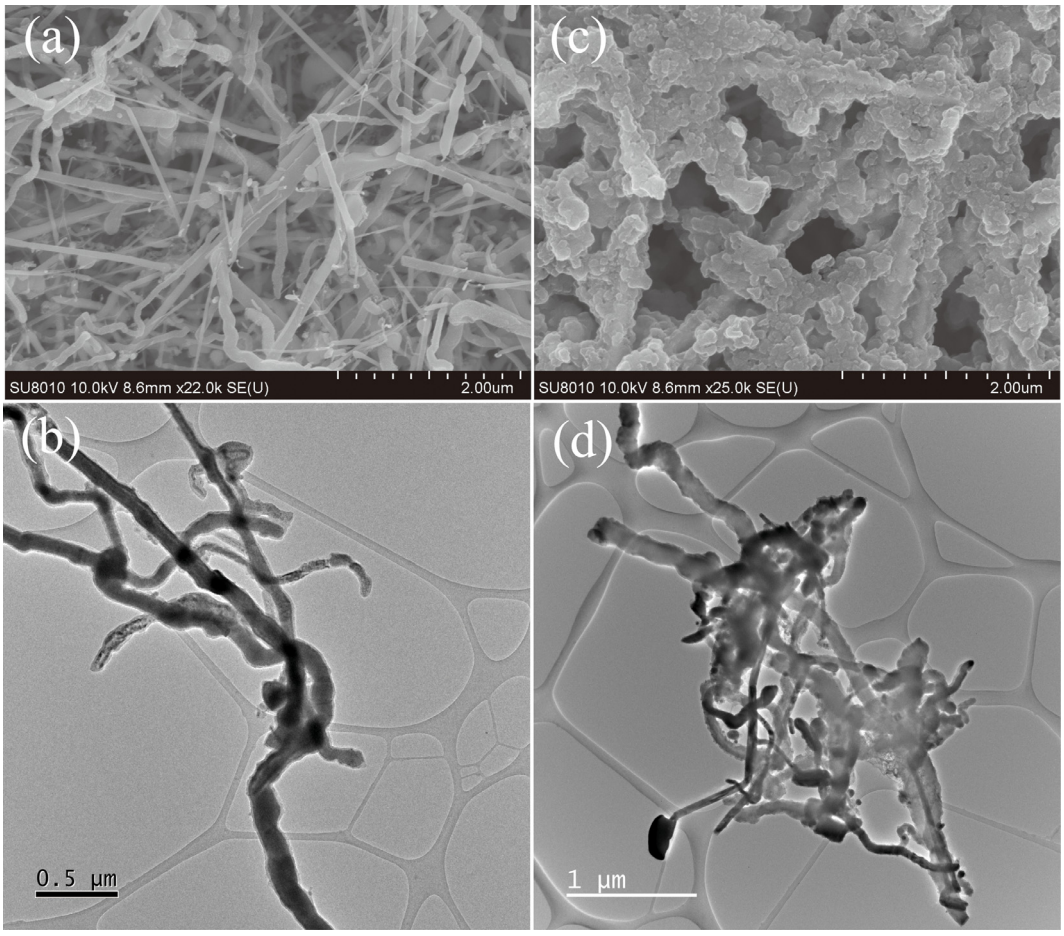

Fig. 11. Si/Cu nanowires of S2 electrode: (a) SEM and (c) TEM images before cycling and (b) SEM and (d) TEM images after cycling.

smaller diameter of the semicircle with fresh cell compared to the ones before cycling, which explains charge transfer resistance decrease. This result again shows that intersection between the Si (Ge) and Cu NWS has a positive effect on electrode conductivities, so as to enhance electron transfer and lithium diffusion in the electrode during cycling (Fig. S6). Nanowire composites can be long-cycling electrodes with optimized parameters for annealing temperatures and Si (Ge)/Cu mixing ratio. For example, the G2 electrode remain its electrochemical performance after 500 cycle at a charge and discharge rate of 1300 mA g^{-1} (Fig. S7).

Figs. 11 and 12 shows high-resolution SEM and TEM images of Si (Ge)/Cu nanowires electrodes before and after 100 cycles. Before cycling, Si and Ge nanowires waved with each other into the fabric structure, as shown in Figs. 11(a) and (b), and 12(a) and (b). X-ray spectroscopy (EDS) of the contact point shows atomic ratio of Cu: Ge is 3:2, which shows the formation of copper germanide. The slight rich of Cu on the contact with respect to Cu_3Ge phase observed in the XRD pattern may be resulted from back scattering of Cu grid. After cycling, nanowire composites were coated with a uniform SEI layer Figs. 11(c) and 12(c). The growth of SEI layer is a well-known phenomenon that occurs during a cycling process. Figs. 11(d) and 12(d) show both Si and Ge nanowires become porous network structure. The network composed of a mass of Si and Ge ligaments and interweave with nearby ligaments and Cu nanowires to form a new work of interconnected porous/solid composites.

In accordance with the above results, two decisive factors determine the electrochemical performance of Si NW/Cu NW fabric electrodes. One is the loading mass of Cu NWs and another is the annealing temperature which are key factors affecting the electrical conductivity of the NW fabric electrodes. The purpose of using Cu NWs in the fabric electrode is to improve the electronic conductivity of the entire fabric electrodes due to the excellent electrical conductivity of Cu. It should be noted that all NWs used for making NW fabric are passivated by organic ligands, therefore, the annealing process can remove the insulating layer on the NW surface. The annealing process also induces the formation of copper silicide (copper germanide) at the intersection between Si (Ge) NWs and Cu NWs, resulting in formatting better contact points and improving electron transport in the NW fabric electrodes (Fig. 13). However, when the loading mass of Cu NWs is too much or thermal annealing temperature is too high, serious Cu diffusion into Si(Ge) leads to destroy the shape of NWs in company with reducing a large number of active materials to form inactive materials resulting in low capacity and poor cycle stability due to loss electrical connections between NWs.

Compared with the previously reported free standing Si NW electrodes, our Si/Cu NW composite battery has a capacity of 1000 mAh/g higher than the carbon-coated Si NW electrode after 50 cycles [27] and is close to the specific capacity of conductive carbon-coated nanowire electrodes [42]. However, the manner in which formation of carbon shell generally requires very high temperatures (> 800 °C). In addition, carbon precursors after thermal decomposition could also produce non-conductive impurities remaining in the electrodes and become a source of side reactions reacted with Li ions, resulting in a Coulomb efficiency less than 50% in the first cycle. Using the method we have reported, the amount of copper nanowires required can be

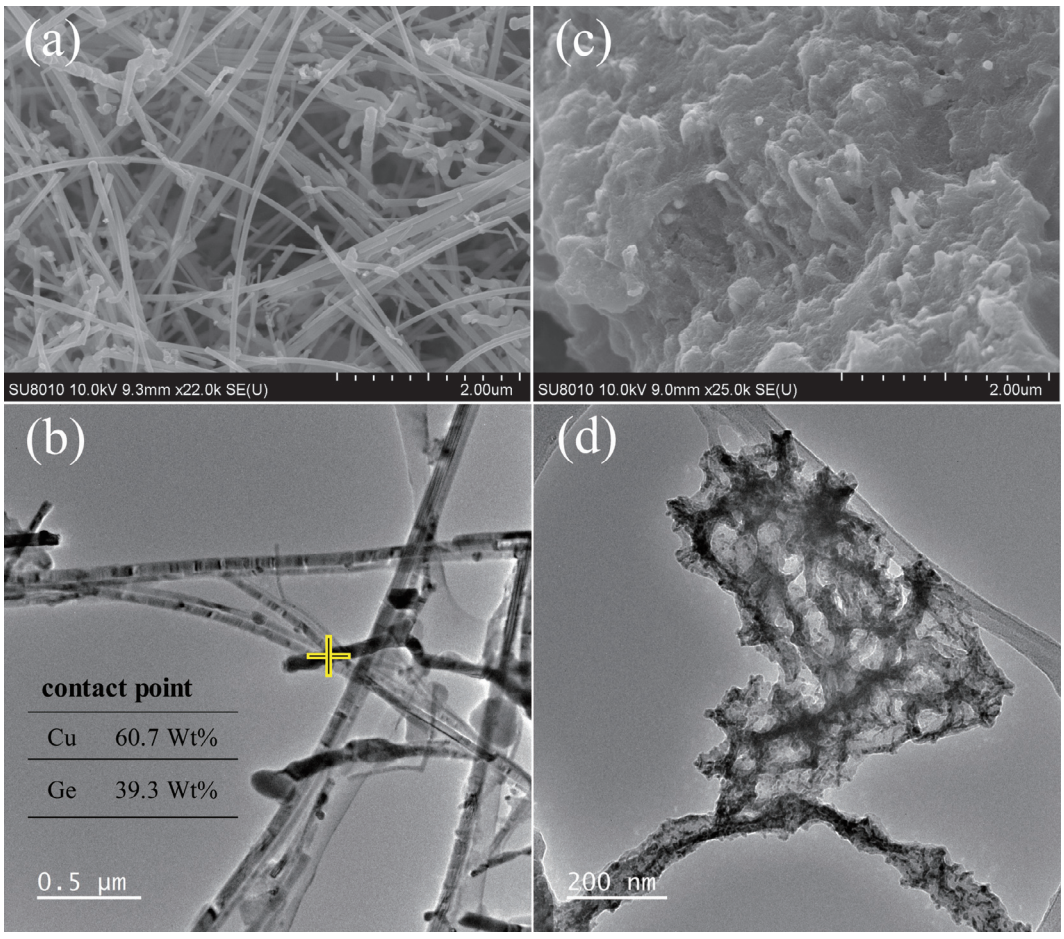

Fig. 12. Ge/Cu nanowires of G2 electrode: (a) SEM and (c) TEM images before cycling and (b) SEM and (d) TEM images after cycling.

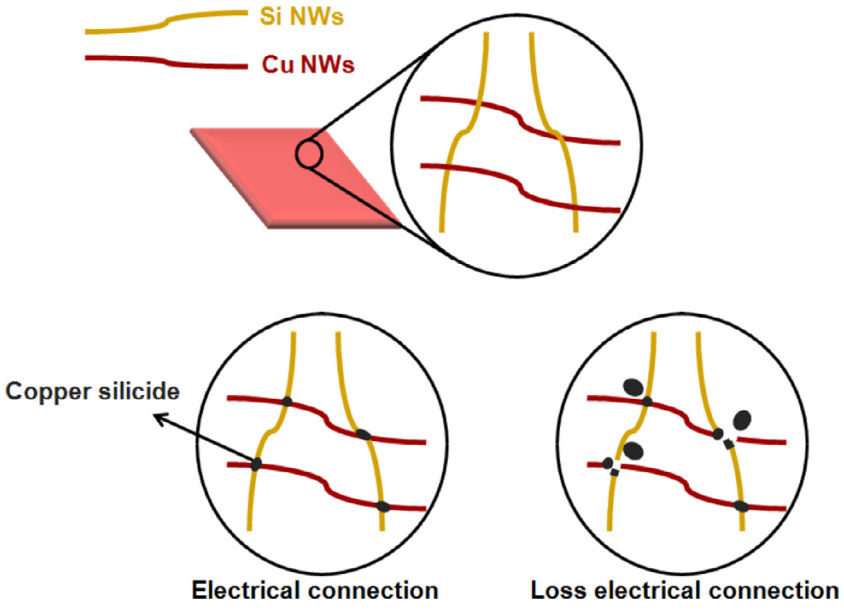

Fig. 13. Schematic diagram of micro-structural changes within the NW fabric after thermal annealing.

precisely controlled and the quality of the electrodes can be easily maintained.

4. Conclusion

In summary, we demonstrate non-carbon based free standing electrodes which are made by high theoretical specific capacity Si (Ge) NWs and high electronic conductivity Cu NWs as LIB anodes. The free standing NW fabric electrodes have some inherent advantages in LIBs application. First, this electrode structure does not need metal foil current collector and addition of polymer binders in the production process, therefore, the weight of whole electrode is significantly lighter than conventional electrodes made by slurry coating on metal foils. Second, the wire shape of the raw materials provides many intersections between NWs (like 3D interconnectivity) resulting in accelerating the electron transport. Third, the space among the NWs can accommodate the volume contraction of Si (Ge) NWs during alloying and dealloying process and enhance the electrolyte penetration leading to Li-ion diffusion in the electrode easier. The loading mass of Cu NWs and the annealing temperature are two decisive factors determining the electrochemical performance of the free standing NW anode electrodes. For example, Si NW/Cu NW fabric electrodes (S2) containing 75 wt% of Cu NW annealing at 500 °C show the best electrochemical performance, whereas Ge NW/Cu NW fabric electrodes (G2) containing 25 wt% of Cu NW annealing at 300 °C. The reported method shows a facile way to improve electrochemical performance of all inorganic nanowire anodes by direct incorporation of metal nanowires into electrode materials. Since the amount of copper nanowires can be precisely controlled and the process is simple, we believe this method can be also beneficial and applicable to other types of alloy-based battery electrodes.

Acknowledgment

We acknowledge the financial support by the Ministry of Science and Technology through the grants of MOST 106- 2221-E-007-081-MY3, MOST 106-2628-E-007-005-MY3, and MOST 103-2221-E-007-089-MY3, and MOST 106-2622-8-007-017, and by National Tsing Hua University through the grant of 107Q2708E1.

Supplementary material

Supplementary material associated with this article can be found, in the online version, at doi:10.1016/j.jtice.2019.07.014.

References

[1] Bruce PG, Scrosati B, Tarascon JM. Nanomaterials for rechargeable lithium batteries. Angew. Chem. Int. Ed. 2008;47:2930–46.
[2] Marom R, Amalraj SF, Leifer N, Jacob D, Aurbach D. A review of advanced and practical lithium battery materials. J. Mater. Chem. 2011;21:9938–54.
[3] He J, Li P, Lv W, Wen K, Chen Y, Zhang W, Li Y, Qin W, He W. Three-dimensional hierarchically structured aerogels constructed with layered MoS2/graphene nanosheets as free-standing anodes for high-performance lithium ion batteries. Electrochimica Acta 2016;215:12–18.
[4] Ji G, Ma Y, Lee JY. Mitigating the initial capacity loss (ICL) problem in high-capacity lithium ion battery anode materials. J. Mater. Chem. 2011;21:9819–24.
[5] Su X, Wu L, Li JC, Xiao XC, Lott A, Lu WQ, Sheldon BW, Wu J. Silicon-based nanomaterials for lithium-ion batteries: a review. Adv. Energ. Mater. 2014;4:1300882.
[6] McDowell MT, Lee SW, Nix WD, Cui Y. Understanding the lithiation of silicon and other alloying anodes for lithium-ion batteries. Adv. Mater. 2013;25:4966–84.
[7] Zhang WJ. A review of the electrochemical performance of alloy anodes for lithium-ion batteries. J. Power Sources 2011;196:13–24.
[8] Cheng FY, Liang J, Tao ZL, Chen J. Functional materials for rechargeable batteries. Adv. Mater. 2011;23:1695–715.
[9] Lee KT, Cho J. Roles of nanosize in lithium reactive nanomaterials for lithium ion batteries. Nano Today 2011;6:28–41.
[10] Chan CK, Peng HL, Liu G, McIlwrath K, Zhang XF, Huggins RA, Cui Y. High-performance lithium battery anodes using silicon nanowires. Nat. Nanotechnol. 2008;3:31–5.
[11] Kim H, Seo M, Park MH, Cho J. A critical size of silicon nano-anodes for lithium rechargeable batteries. Angew. Chem. Int. Edit. 2010;49:2146–9.
[12] Park MH, Cho Y, Kim K, Kim J, Liu ML, Cho J. Germanium Nanotubes Prepared by Using the Kirkendall Effect as Anodes for High-Rate Lithium Batteries. Angew. Chem. Int. Edit. 2011;50:9647–50.
[13] Park MH, Kim K, Kim J, Cho J. Flexible dimensional control of high-capacity li-ion-battery anodes: from 0D hollow to 3D porous germanium nanoparticle assemblies. Adv. Mater. 2010;22:415.
[14] Park MH, Kim MG, Joo J, Kim K, Kim J, Ahn S, Cui Y, Cho J. Silicon nanotube battery anodes. Nano. Lett. 2009;9:3844–7.
[15] Tan LP, Lu ZY, Tan HT, Zhu JX, Rui XH, Yan QY, Hng HH. Germanium nanowires-based carbon composite as anodes for lithium-ion batteries. J. Power Sources 2012;206:253–8.
[16] Chan CK, Zhang XF, Cui Y. High capacity Li ion battery anodes using Ge nanowires. Nano. Lett. 2008;8:307–9.
[17] Zhang Q, Chen H, Luo L, Zhao B, Luo H, Han X, Wang J, Wang C, Yang Y, Zhu T, Liu Meilin. Harnessing the concurrent reaction dynamics in active Si and Ge to achieve high performance lithium-ion batteries. Energ. Environ. Sci. 2018;11:669–81.
[18] Serino AC, Ko JS, Yeung MT, Schwartz JJ, Kang CB, Tolbert SH, Kaner RB, Dunn BS, Weiss PS. Lithium-Ion Insertion Properties of Solution-Exfoliated Germanane. ACS Nano 2017;11:7995–8001.
[19] Liu Z, Guan D, Yu Q, Xu L, Zhuang Z, Zhu T, Zhao D, Zhou L, Mai L. Monodisperse and homogeneous SiOx/C microspheres: A promising high-capacity and durable anode material for lithium-ion batteries. Energy Storage Mater 2018;13:112–18.
[20] Liu Z, Yu Q, Zhao Y, He R, Xu M, Feng S, Li S, Zhou L, Mai LS. Silicon oxides: a promising family of anode materials for lithium-ion batteries. Chem. Soc. Rev. 2019;48:285–309.
[21] Chew SY, Ng SH, Wang JZ, Novak P, Krumeich F, Chou SL, Chen J, Liu HK. Flexible free-standing carbon nanotube films for model lithium-ion batteries. Carbon 2009;47:2976–83.
[22] Wang CY, Li D, Too CO, Wallace GG. Electrochemical properties of graphene paper electrodes used in lithium batteries. Chem. Mater. 2009;21:2604–2606.
[23] Chou SL, Zhao Y, Wang JZ, Chen ZX, Liu HK, Dou SX. Electrochemical properties of graphene paper electrodes used in lithium batteries. J. Phys. Chem. C 2010;114:15862–7.
[24] Yuan FW, Tuan HY. Scalable solution-grown high-germanium-nanoparticle-loading graphene nanocomposites as high-performance lithium-ion battery electrodes: an example of a graphene-based platform toward practical full-cell applications. Chem. Mater. 2014;26:2172–9.
[25] Wang J, Wang G, Wang H. Flexible free-standing Fe2O3/graphene/carbon nanotubes hybrid films as anode materials for high performance lithium-ion batteries. Electrochimica Acta 2015;182:192–201.
[26] Wang JG, Jin D, Zhou R, Li X, Liu XR, Shen C, Xie K, Li B, Kang F, Wei B. Highly flexible graphene/Mn3O4 nanocomposite membrane as advanced anodes for li-ion batteries. ACS nano 2016;10:6227–34.
[27] Chockla AM, Harris JT, Akhavan VA, Bogart TD, Holmberg VC, Steinhagen C, Mullins CB, Stevenson KJ, Korgel BA. Silicon nanowire fabric as a lithium ion battery electrode material. J. Am. Chem. Soc. 2011;133:20914–21.
[28] Chang WC, Kao TL, Lin Y, Tuan HY. A flexible all inorganic nanowire bilayer mesh as a high-performance lithium-ion battery anode. J. Mater. Chem. A 2017;5:22662–71.
[29] Yuan FW, Yang HJ, Tuan HY. Alkanethiol-passivated Ge nanowires as high-performance anode materials for lithium-ion batteries: the role of chemical surface functionalization. ACS Nano 2012;6:9932–42.
[30] Brust M, Walker M, Bethell D, Schiffrin DJ, Whyman R. Synthesis of thiol-derivatised gold nanoparticles in a two-phase liquid–liquid system. Chem. Comm. 1994:801–2.
[31] Yang HJ, He SY, Tuan HY. Self-seeded growth of five-fold twinned copper nanowires: mechanistic study, characterization, and SERS applications. Langmuir 2014;30:602–10.
[32] Liu BR, Soares P, Checkles C, Zhao Y, Yu GH. Three-dimensional hierarchical ternary nanostructures for high-performance Li-ion battery anodes. Nano Lett 2013;13:3414–19.
[33] Kong JH, Yee WA, Wei YF, Yang LP, Ang JM, Phua SL, Wong SY, Zhou R, Dong YL, Li X, Lu XH. Silicon nanoparticles encapsulated in hollow graphitized carbon nanofibers for lithium ion battery anodes. Nanoscale 2013;5:2967–2973.
[34] Wang JZ, Du N, Zhang H, Yu JX, Yang DR. Cu–Ge core–shell nanowire arrays as three-dimensional electrodes for high-rate capability lithium-ion batteries. J. Mater. Chem. 2012;22:1511–15.
[35] Zhong C, Wang JZ, Gao XW, Wexler D, Liu HK. In situ one-step synthesis of a 3D nanostructured germanium–graphene composite and its application in lithium-ion batteries. J. Mater. Chem. A 2013;1:10798–804.
[36] Chockla AM, Klavetter KC, Mullins CB, Korgel BA. Solution-grown germanium nanowire anodes for lithium-ion batteries. ACS Appl. Mater. Inter. 2012;4:4658–64.
[37] Etacheri V, Haik O, Goffer Y, Roberts GA, Stefan IC, Fasching R, Aurbach D. Effect of fluoroethylene carbonate (FEC) on the performance and surface chemistry of Si-nanowire Li-ion battery anodes. Langmuir 2012;28:965–976.
[38] Chae OB, Park S, Ku JH, Ryu JH, Oh SM. Nano-scale uniform distribution of Ge/Cu3Ge phase and its electrochemical performance for lithium-ion batteries. Electrochim Acta 2010;55:2894–900.

[39] Chen HX, Xiao Y, Wang L, Yang Y. Silicon nanowires coated with copper layer as anode materials for lithium-ion batteries. J. Power Sources 2011;196:6657–62.
[40] He Y, Wang YH, Yu XQ, Li H, Huang XJ. Si-Cu thin film electrode with Kirkendall voids structure for lithium-ion batteries. J. Electrochem. Soc. 2012;159:A2076–81.
[41] Kim JH, Kim H, Sohn HJ. Addition of Cu for carbon coated Si-based composites as anode materials for lithium-ion batteries. Electrochem. Commun. 2005;7:557–61.
[42] Bogart TD, Oka D, Lu XT, Gu M, Wang CM, Korgel BA. Lithium ion battery performance of silicon nanowires with carbon skin. ACS Nano 2014;8:915–22.